Carbon 115 (2017) 819–827

Contents lists available at ScienceDirect

Carbon

journal homepage: www.elsevier.com/locate/carbon

Study of the cap structure of (3,3), (4,4) and (5,5)-SWCNTs: Application of the sphere-in-contact model

Constantinos D. Zeinalipour-Yazdi [a, *], Eriketi Z. Loizidou [b]

[a] Kathleen Lonsdale Materials Chemistry, Department of Chemistry, University College London, London, WC1H 0AJ, UK
[b] Department of Natural Sciences, Middlesex University Hendon Campus, The Burroughs, London, NW4 4BT, UK

ARTICLE INFO

Article history:
Received 7 November 2016
Received in revised form
3 January 2017
Accepted 23 January 2017
Available online 26 January 2017

Keywords:
SWCNT
Carbon nanotube
Cap structure
Sphere-in-contact model
DFT

ABSTRACT

We have applied the sphere-in-contact model supported by hybrid Density Functional Theory (DFT) calculations to elucidate the cap geometry of the sub-nanometer in dimension (3,3), (4,4) and (5,5) single-wall carbon-nanotubes (SWCNTs). Our approach predicts certain cap-geometries that do not comprise of the commonly known for their stability combination of pentagonal and hexagonal carbon rings but also tetragonal, trigonal and all-pentagonal structures. Based on hybrid-DFT calculations carbon atoms in these new cap geometries have similar stability to carbon found in other fullerene-like capped zig-zag and arm-chair nanotubes (i.e., (5,5), (6,6), (9,0) and (10,0)) that are known to be stable and synthetically accessible. We find that the cap structure of the (3,3)-CNTs is a pointy carbon geometry comprised of six pentagonal rings with a single carbon atom at the tip apex. In this tip geometry the carbon atom at the tip apex does not have the usual sp^2 or sp^3 geometry but an unusual trigonal pyramidal configuration. DFT calculations of the molecular orbitals and density-of-states of the tip show that this tip structure apart from being stable can be used in scanning probe microscopies such as STM for very high resolution imaging.

1. Introduction

Scanning probe microscopy (SPM) instruments have been very popular in research since the discovery of the Scanning Tunneling Microscope (STM) in the 80's. There has been an increased amount of research over the last three decades to increase the resolution of these instruments from several nanometers to sub-nanometer resolution, either by vibrational isolation of the SPM head or by modification of the tip composition and structure. Carbon nanotubes (CNT) attached to commonly used tips in STM, such as W or Pt/Ir probes, have been suggested as a way to improve the resolution of topographic imaging to sub-nanometer resolution. In atomic-force microscopy (AFM) they enable high resolution measurements and manipulation when in tapping-mode [1]. The large aspect ratio, high mechanical strength and chemical stability of CNT modified SPM probes makes them suitable for measurements where sub-nanometer resolution is necessary [2]. The CNT-modified STM tips have been shown to be superior than the typical W-tips used for measuring the square profile of gratings [3].

Controlled synthesis of CNTs belonging to particular chiral index (*n*,*m*) has recently been achieved via cyclodehydrogenation of a polycyclic polyaromatic hydrocarbon (PAH) (i.e. $C_{96}H_{54}$) on Pt substrates [4]. The cap of single-walled carbon nanotube (SWCNT) such as the zig-zag (9,0)-CNT and arm-chair (6,6)-CNT can be synthesized using surface-assisted cyclo-dehydrogenation of $C_{54}H_{24}$ and $C_{60}H_{30}$, respectively, on rhodium-(111) surfaces with thermal stabilities up to 820 K, appropriate for subsequent SWCNT growth [5]. Miyauchi et al. suggested that the cap geometry is mostly important in determining the chirality of the CNT when grown via chemical-vapor-deposition (CVD). Fabrication of ultra-sharp carbon fiber (CF) tips have recently been used in dynamic-STM and frequency-modulation AFM experiments [6]. The electron transport properties using Green's function approach showed that fullerene/metal electrode have resonant states near the Fermi level, indicative of better electron transport properties in fullerene functionalised or capped CNT tips [7,8]. It is therefore useful to know the stable cap geometry of the smaller in diameter SWCNTs (e.g. (3,3) and (4,4)) as such capped SWCNT could serve as potential high resolution probes in STM and AFM. The structural identification of the cap geometry has been relied on graphical and computational algorithms to identify the cap structure of minimum energy for a SWCNT of a given chirality (*n*,*m*). Graphical approaches

* Corresponding author.
E-mail address: c.zeinalipour-yazdi@ucl.ac.uk (C.D. Zeinalipour-Yazdi).

http://dx.doi.org/10.1016/j.carbon.2017.01.074

place hexagons, pentagons and heptagons on a curved surface in order to form fullerene-like structures [9,10]. Recently, there has been a numerical method that makes use of the solution of the Thomson problem [11] that distributes point charges on a sphere [12] in order to identify the location of carbon rings. In this paper we have used a physical sphere-in-contact models [13] and hybrid-DFT calculations, to elucidate the stable arrangement of the cap in a various SWCNT of known geometry and for the unknown in structure (3,3), (4,4) and (5,5)-SWCNTs.

First, we present via density-of-states (DOS) and molecular-orbital (MO) plots that sub-nanometer SWCNT can be used as STM tips for sub-nanometer resolution. Then via physical sphere-in-contact models we determine possible cap structures for the (3,3), (4,4) and (5,5)-SWCNTs. Based on average bond-dissociation-enthalpies (BDE) we compare the stability of the new cap structures to the stability of other known carbon materials (e.g. fullerene, graphene nanoribbons (GNR), carbon nanocones). Finally, we present MO and DOS plots of these new carbon geometries in order to show that they can be used in STM.

2. Methods

2.1. Computational methods

We have energetically optimised the atomic positions of the carbon materials with DFT computations implemented Gaussian09 (rev D.01) [14]. The zig-zag or arm-chair edge of these carbon materials was saturated with hydrogen atoms in order to fill the dangling edge states. In order to reduce the computational requirements, the CNT structures were constrained within their highest point-group symmetry. The exchange and correlation (XC) effects were considered within the generalized gradient approximation (GGA) with Becke's three-parameter, hybrid exchange functional [15] combined with the Lee-Yang-Parr non-local correlation functional [16], abbreviated as B3LYP. For the calculations the standard molecular basis sets STO-3G, 6-31G(d) and cc-pVDZ have been adopted to test the convergence of the basis set, for which the same trends were found and therefore only the cc-pVDZ results are reported. However, energetic minima of the various SWCNTs were confirmed by vibrational analysis using the STO-3G basis set in order to reduce the computational requirements for evaluating the Hessian. These calculations confirmed an absence of imaginary vibrational frequency modes for the minimum structures. The optimisation parameters resulted in maximum forces and the root-mean-square (RMS) of the forces to be less than 0.01 eV/Å and 0.001 eV/Å, respectively.

2.2. Materials

The initial sphere-in-contact models were constructed using marbles and epoxy-glue. We later found that Aquabeads (or Beados) can be readily turned into inexpensive physical models of carbon nanotubes in a short amount of time. For the physical sphere-in-contact models made out of marbles and epoxy-glue we have used about 150 glass marbles (14 mm) that were bound with epoxy resin adhesive. The models were placed on a rectangular sheet of Poly(methyl)-methacrylate (PMMA). A detailed description of the procedure is given in Section 3.3.

3. Results and discussion

3.1. Electronic structure of tubular and capped SWCNT

The use of CNT has been mostly in applications where bundles [17], composites (e.g. multifunctional CNT reinforced nanocomposites [18,19]), random networks (e.g. buckypaper-films [20]) of CNT or CNT-supported metal nanoparticles (e.g. Ag-NP supported CNTs [21]) offer new properties. However, there are very few technological applications that utilise isolated CNTs. In this section we explore some of the electronic properties of tubular and capped SWCNT in order to show that they exhibit certain features, which make them suitable as STM probes.

In Fig. 1 the highest occupied MO (HOMO) and the lowest unoccupied MO (LUMO) and the corresponding DOS of a tubular and capped (4,4)-CNT, are shown. On one hand, the tubular (4,4)-SWCNT have semi-metallic electronic properties (see Fig. 1c) seen by the valence and conduction band cone at the Fermi level. The absence of states near the Fermi level makes tubular SWCNTs less suitable in their use as STM probes as they lack availability of states that could enhance the tunneling current, due to protruding orbitals in the tip-to-surface vacuum gap. On the other hand, the capped (4,4)-SWCNT (Fig. 1b) has an overlap between the valence and conduction band due to additional states close to the Fermi level, which indicates the possibility of conduction of the HOMO into empty states of the conduction band of the SWCNT and from there into empty states of the conducting surface, in the case of STM. This can also be observed in the enhanced DOS at the Fermi level shown in Fig. 1d in contrast to the DOS of the tubular SWCNT that is zero at the Fermi level, shown in Fig. 1c. Hence, we show that capped sub-nanometer SWCNTs are expected to have better electron transport properties than the hydrogen functionalised tubular SWCNTs. However, the cap geometry of this (4,4)-SWCNT is such that four orbitals have protruding orbitals in the tip-to-surface vacuum gap, which could result in a multiple-tip effect in STM. In the last section we show that the HOMO of the new cap structure of the (3,3)-SWCNT protrudes into the vacuum gap by a single orbital rather than multiple distribution observed on tubular hydrogen functionalised SWCNTs and on capped SWCNT of different chiral index.

3.2. Cap structure of low index SWCNTs

There are several computer graphics programs used for the design of SWCNTs of certain chirality (n,m) and length. Typical software only generate the structure of the cap for SWCNT with certain low-index pre-determined chiralities. We have used NanoTube modeler [23] to design two zig-zag (i.e., (5,5), (6,6)) and two arm-chair nanotubes (i.e., (9,0) and (10,0)) SWCNT of known cap geometry. The stability of the carbon atoms in these structures was compared to the stability of the carbon atoms in new tip structures where the geometry was determined via sphere-in-contact models. With this approach we found that there are two possible cap geometries for each sub-nanometer (n,n)-CNT, where $n = 3$, 4 and 5.

In Fig. 2 we present the structure of the smallest in diameter carbon nanotubes of such nanotubes with their most stable cap for two arm-chair (i.e., (5,5) and (6,6)) and two zig-zag (i.e., (9,0) and (10,0)) SWCNTs. These were drawn in the commonly used ball-and-stick model representation and compared to sphere-in-contact representation for carbon materials [13]. The dangling bond edge states of these SWCNTs was saturated with one H-atom for each carbon atom at the edge of the SWCNT, in order to increase their stability. In Fig. 2 we show that the cap of these CNTs is represented with great accuracy within the sphere-in-contact model, based on how well the sphere touch when the radius of carbon is equal to carbon's covalent radius (i.e. 0.71 pm). These cap structures have been previously found to be stable at the semi-empirical AM1 level of theory [9]. They comprised of all pentagon and hexagon structures with either a pentagonal (e.g. (5,5), (10,0)) or a hexagonal (e.g. (6,6), (9,0)) carbon ring at the tip apex.

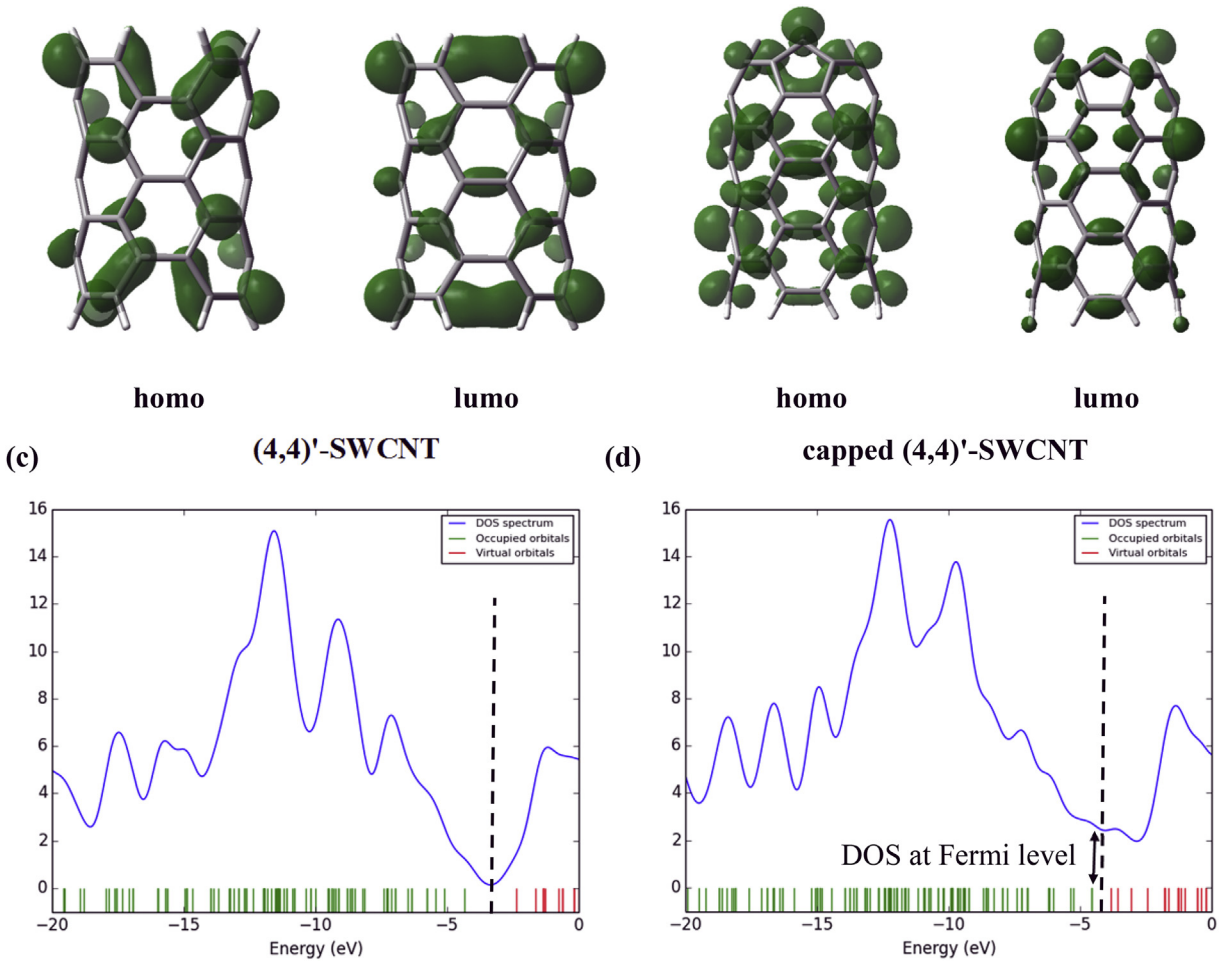

Fig. 1. (a)–(c) HOMO-LUMO and DOS plots of (4,4)'-CNT and (b)–(d) HOMO-LUMO and DOS of capped (4,4)'-CNT. Energy levels were fit with gaussian functions of full-width-at-half-maximum, (FWHM) of 1eV. In the capped nanotube there is an overlap between valence and conduction band, indicative of better conductivity in capped CNTs due to protruding WF in the vacuum gap. Dashed line indicates Fermi level. DOS plots generated in Gausssum [22]. (A colour version of this figure can be viewed online.)

3.3. Construction of sphere-in-contact model of capped SWCNTs

In this section we present a procedure to construct physical sphere-in-contact model of a capped (4,4)-SWCNT. A pictorial procedure of this nanotube is given in Fig. 3. The spheres were initially glued on the curved surface of a paper cylinder that had a diameter of 53 mm. The procedure was the following: (i) The paper cylinder was placed vertically and spheres (i.e. marbles) were bound to the paper cylinder with the use of a hot glue dispenser; 12 marbles completed the perimeter of the first carbon ring; then we applied epoxy-glue, which was thoroughly mixed by means of a disposable spatula, and placed at the contact point between the marbles; only every third C—C should was glued this way and once the first layers had dried, which took 2 min with fast drying epoxy-resins, we then removed the carbon atoms that were not bound; (ii) we then repeated step-i as many times necessary in order to obtain the tubular part of the SWCNT; (iii) once the SWCNT cylinder was constructed the supporting inner paper cylinder was removed by pressing it with the back site of a pen, through the hexagonal rings; the compressed paper cylinder can then be pulled out of the SWCNT cylinder; (iv) the cap can be constructed via a similar process, in which a supportive hemisphere made out of polystyrene is first placed at one end of the cylinder; (v) the procedure was very similar to step-i for the first ring; (vi) for the second ring only four carbon atoms were placed at the gap formed by four pairs of carbon atoms, forming four five-member carbon rings; (vii) at the CNT tip there is only room for one more marble, which forms a single carbon atom at the tip apex; (viii) we then removed the polystyrene hemisphere by pushing the back side of a pen through the four carbon rings formed at the tip of the CNT; (ix) the last step was to place this CNT onto a PMMA sheet and attach labels to the model that show the name and scale (i.e. (4,4)-SWCNT scale $1{:}10^8$) of the capped (4,4)-SWCNT model.

3.4. Elucidation of cap geometry of (3,3), (4,4) and (5,5)-CNTs

As the models constructed in Section 3.3 are not practical to explore other geometries for these structures, we have found a way to construct these structures from Aquabeads (or Beados). These are 5 mm in diameter plastic beads that when brought in contact with water initially swell, and later after drying due to water evaporation, the contact points between the spheres bind, forming semi-flexible C—C bonds. We found that with these spheres we can construct very accurate physical models of carbon materials (e.g. CNTs, NC, graphene etc) and can explore alternative structures for the cap geometry. These beads have the additional advantage that they do not need to be glued together via epoxy-glue or super-glue which can be tedious. Aquabead (or Beados) sets are rather inexpensive (600 beads can cost about 4GBP) and they are usually supplied with a hexagonal grid, which restricts the lateral movement of the beads when placed in a hexagonal array. We were able to construct carbon sheets of various shapes for low-chirality CNTs

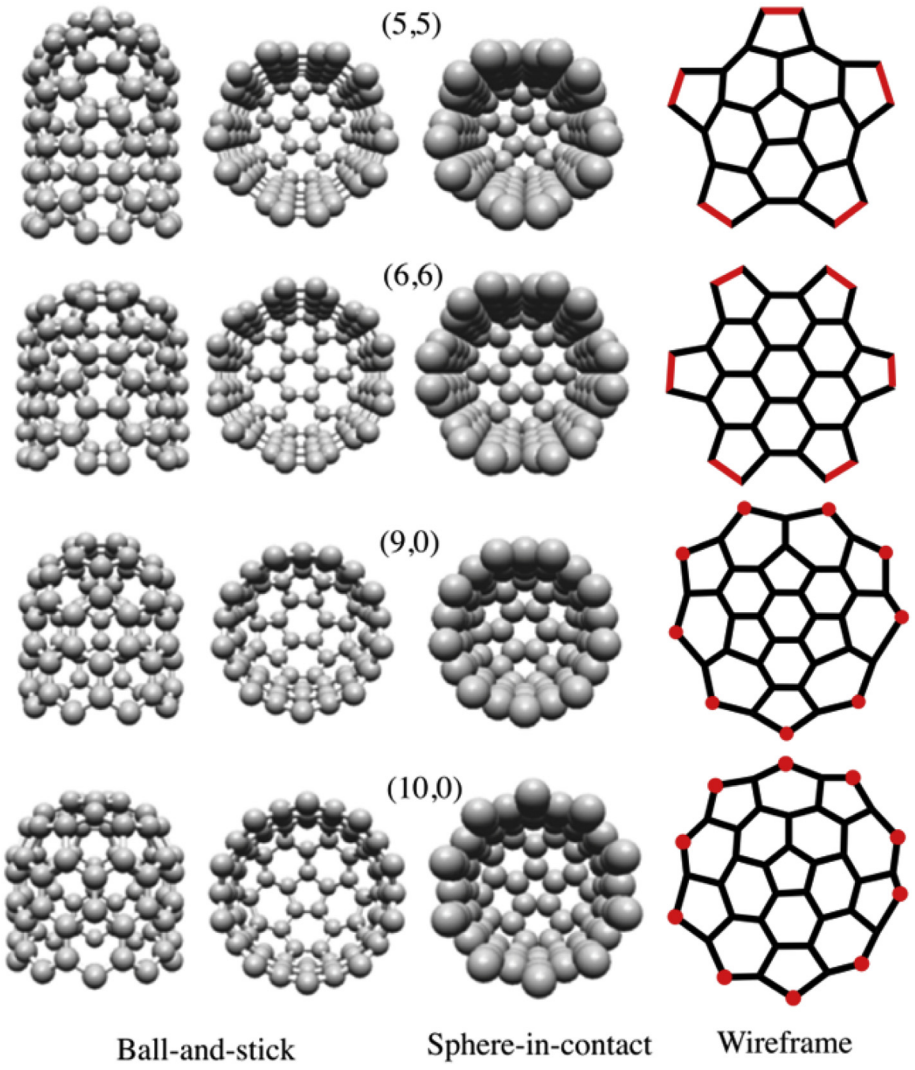

Fig. 2. (a) Arm-chair (5,5)-CNT, (b) arm-chair (6,6)-CNT, (c) zig-zag (9,0)-CNT and (d) zig-zag (10,0)-CNT in ball-and-stick (i.e. side and top view), sphere-in-contact and 2D-wireframe representations of the cap connectivity. Red dot and line indicate atoms that are bound to the SWCNT. Structures drawn with Nanotube Modeller [23]. (A colour version of this figure can be viewed online.)

in just a few minutes. Once the graphene sheets were made and dried, they were rolled on a cylindrical object (e.g. pen) in order to bring the zig-zag edges in contact and bind them with super-glue.

With this procedure we found the cap geometry of various sub-nanometer in width SWCNTs. The side and top view of the various possible geometries for the (3,3), (4,4) and (5,5)-SWCNTs are shown in Figs. 4 and 5 (shown in Appendix A), respectively. We report only geometries where the spheres were in good contact, as the other would not be stable according to the empirical property that stable covalent bonds are formed only when the spheres of atomic (i.e. covalent) radius are in perfect contact. In particular we found that there are two stable cap geometries denoted as (*n,n*) and (*n,n*)' for each (*n,n*)-SWCNT, where n = 3, 4 and 5.

3.5. Stability measurement of carbon in cap geometry via BDE calculation

In the previous section we have shown that we can construct the model of carbon nanotubes and their cap geometry very easily without detailed trigonometric derivations. Their stability was assessed in this section via hybrid-DFT calculations. Since the stability of two atoms bound through a chemical bond can be assessed by calculating the bond dissociation enthalpy (BDE) we have therefore evaluated the average BDE for various stable carbon materials (i.e. fullerene, GNR) and compared it to that of the new cap structures found with the sphere-in-contact models.

The bond dissociation enthalpy of a PAH was calculated based on the following equation

$$av.BDE_{PAH} = E_{PAH} - n_C E_C - n_H E_H + ZPV_{PAH} \quad (1)$$

where n_C and n_H is the number of C and H atoms, respectively. E_{PAH}, E_C and E_H are the total energies of the PAH, of an isolated carbon atom in its triplet state and a hydrogen atom in its doublet state and the zero-point vibrational energy (ZPV_{PAH}) was calculated based on,

$$ZPV_{PAH} \cong \frac{h}{2}\left(\sum_{i=1}^{n_{CC}} v_{CC,i} + \sum_{j=1}^{n_{CH}} v_{CH,j}\right) \quad (2)$$

where n_{CC} and n_{CH} are the number of C–C and C–H bonds, respectively. Furthermore $v_{CC,i}$ and $v_{CH,j}$ are the vibrational energies of the bonds i and j, respectively, which were calculated via the

Fig. 3. (a) Sphere-in-contact model (i.e. paper cylinder ⌀ = 53 mm, 133 × 14 mm marbles, super or epoxy glue) of (4,4)-CNT and (b) pictorial procedure for the construction of it. Note that there is one more tip geometry which was found to be more stable and is depicted in Fig. 4. (A colour version of this figure can be viewed online.)

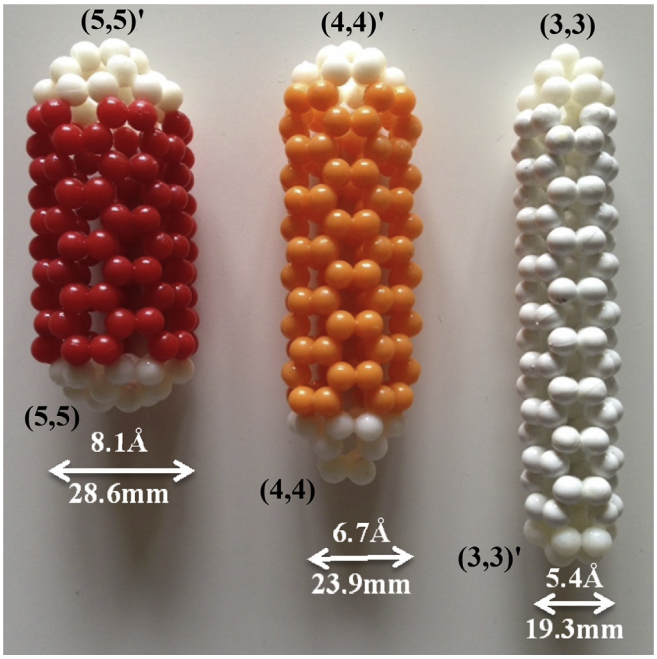

Fig. 4. Side-view of (a) sphere-in-contact model of various capped arm-chair (*m*,*n*)-CNTs where $m = n = 3$, 4 and 5 made out of Aquabeads where $r_C = 2.5$ mm. (A colour version of this figure can be viewed online.)

harmonic oscillator approximation and the finite-difference method. The average BDE per C–C bond was calculated based on the following relationship,

$$av.BDE_{CC} = \frac{BDE_{PAH} - n_{CH} \cdot BDE_{CH}}{n_{CC}} \tag{3}$$

where BDE_{CH} is the average bond-dissociation energy of the C–H bond, n_{CH} and n_{CC} the number of C–H and C–C bonds in the PAH.

Therefore, after combination of equations (1)–(3), the average BDE per C–C bond in an arbitrary PAH becomes,

$$av.BDE_{CC} = \frac{1}{n_{CC}} \left[E_{PAH} - n_C E_C - n_H E_H + \frac{h}{4\pi} \left(\sum_{i=1}^{n_{CC}} \nu_{CC,i} + \sum_{j=1}^{n_{CH}} \nu_{CH,j} \right) - n_{CH} \cdot BDE_{CH} \right]. \tag{4}$$

The BDE_{CH} was estimated based on the energy required to dissociate a hydrogen atom from coronene ($R = C_{24}H_{12}$) forming the corresponding radical ($R^{\bullet} = C_{24}H_{11}^{\bullet}$) given by

$$BDE_{CH} = E_{RH} - E_{R\cdot} - E_{H^+} + ZPV_{CH} \tag{5}$$

The average BDE_{CH} for coronene at B3LYP/cc-pVDZ(5d,7f) level of theory was found to be 454 kJ/mol comparable to value reported for the BDE_{CH} in benzene 473 and methane 439 [24]. The zero-point vibrational energy (ZPV) of C–H at the same level of theory was

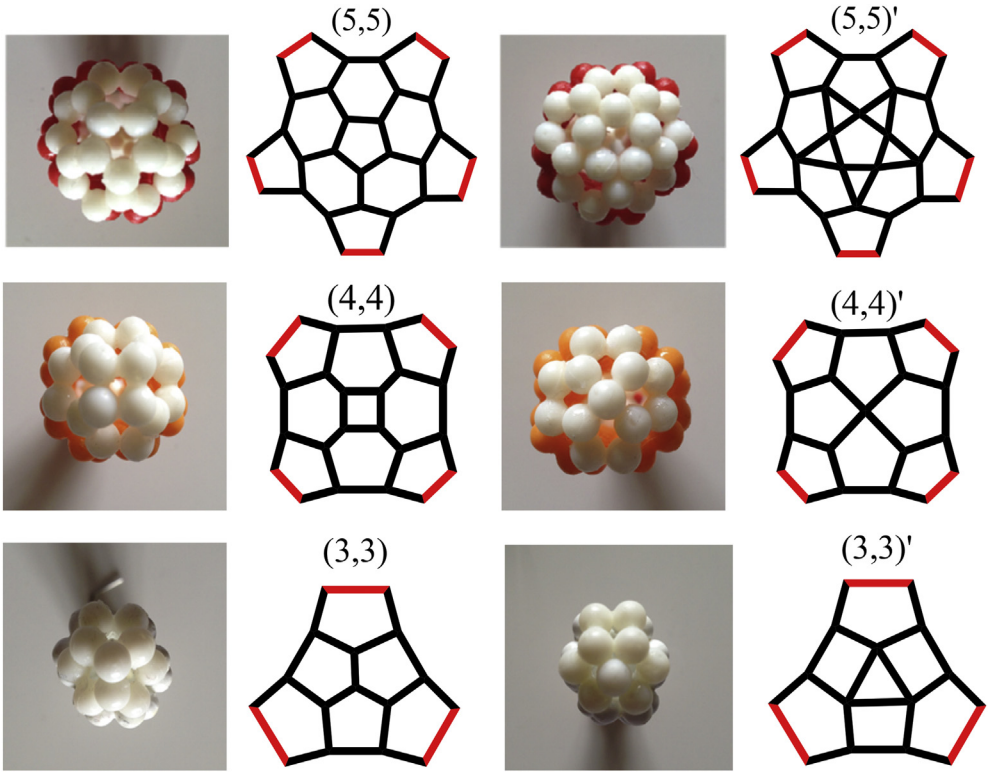

Fig. 5. Top-view of sphere-in-contact models and 2D-wireframe presentations of the (3,3), (4,4) and (5,5)-SWCNT made of Aquabeads (or Beados) in which $r_C = 2.5$ mm. There are two possible structures for each (*n*,*n*)-SWCNT. (A colour version of this figure can be viewed online.)

found to be 34 kJ/mol in excellent agreement with the zero-point energy (ZPE) 36 kJ/mol, calculated from the IR band of the C–H stretching in PAHs located between 3000 and 3100 cm^{-1} [25], with the formula given by,

$$ZPE = \hbar\frac{\omega}{2}. \quad (6)$$

The ZPV of C–H was calculated with the following equation,

$$ZPV_{CH} = ZPV_{RH} - ZPV_{R\cdot} \quad (7)$$

where ZPV_{RH} and $ZPV_{R\cdot}$ are the zero-point vibrational energy of coronene and the coronene radical in its triplet state calculated at B3YP/cc-pVDZ(5d,7f), respectively.

The average BDE of various stable carbon structures and the capped-SWCNT are shown Fig. 6. These calculations show that the stability of planar carbon materials is higher than carbon materials with curved surfaces (e.g. Fullerenes, NC and CNTs). This is associated to the existence of the energy requirements to bend a GNR [26]. The bending energy is considerably smaller that the shearing and compression energy as we have previously shown for GNR of varying size [26]. Noteworthy, is that the average BDE is correlated

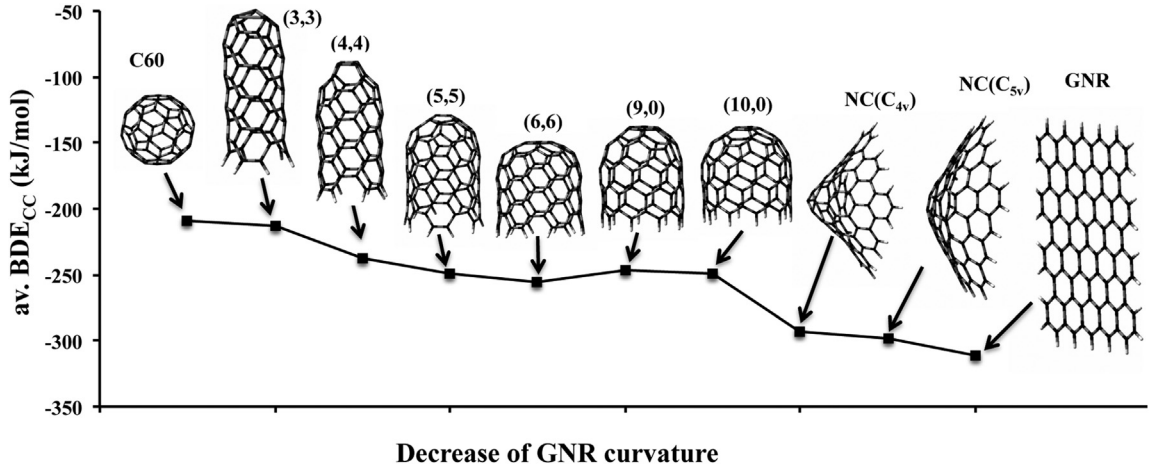

Fig. 6. Stability trends of various carbon materials based on the average BDE of the C-C bond calculated by Eqn. (4) as a function of their curvature. Calculations made at B3LYP/cc-pVDZ (5d, 7f) level of theory.

to the degree of curvature in the average BDE of the materials shown in Fig. 6. GNR has the highest in absolute value av. BDE due to its planar structure. The stability of the carbon atoms in this structure is therefore the greatest among the carbon materials examined. This is followed by nanocones (NC) whose energy increase is inversely proportional to the tip angle, defined by one of the vertical mirror planes of the C_{5v} and C_{4v} point-group symmetry, respectively. The stability of the capped-SWCNT we have examined is intermediate between that of fullerene and the NCs. The most stable capped-SWCNT based on the calculated av. BDE was the capped (6,6)-SWCNT whereas the least stable was the capped (3,3)-SWCNT due to an increased curvature at the tip apex. The relative stability trends of the arm-chair SWCNTs (3,3), (4,4), (5,5) and (6,6)-CNTs appears to be a function of the SWCNT and cap curvature. This trend can also be seen to a smaller extent for the zig-zag capped SWCNTs (9,0) and (10,0). These results clearly indicate that the cap geometries found with the sphere-in-contact models are stable and therefore the sphere-in-contact models were successful in

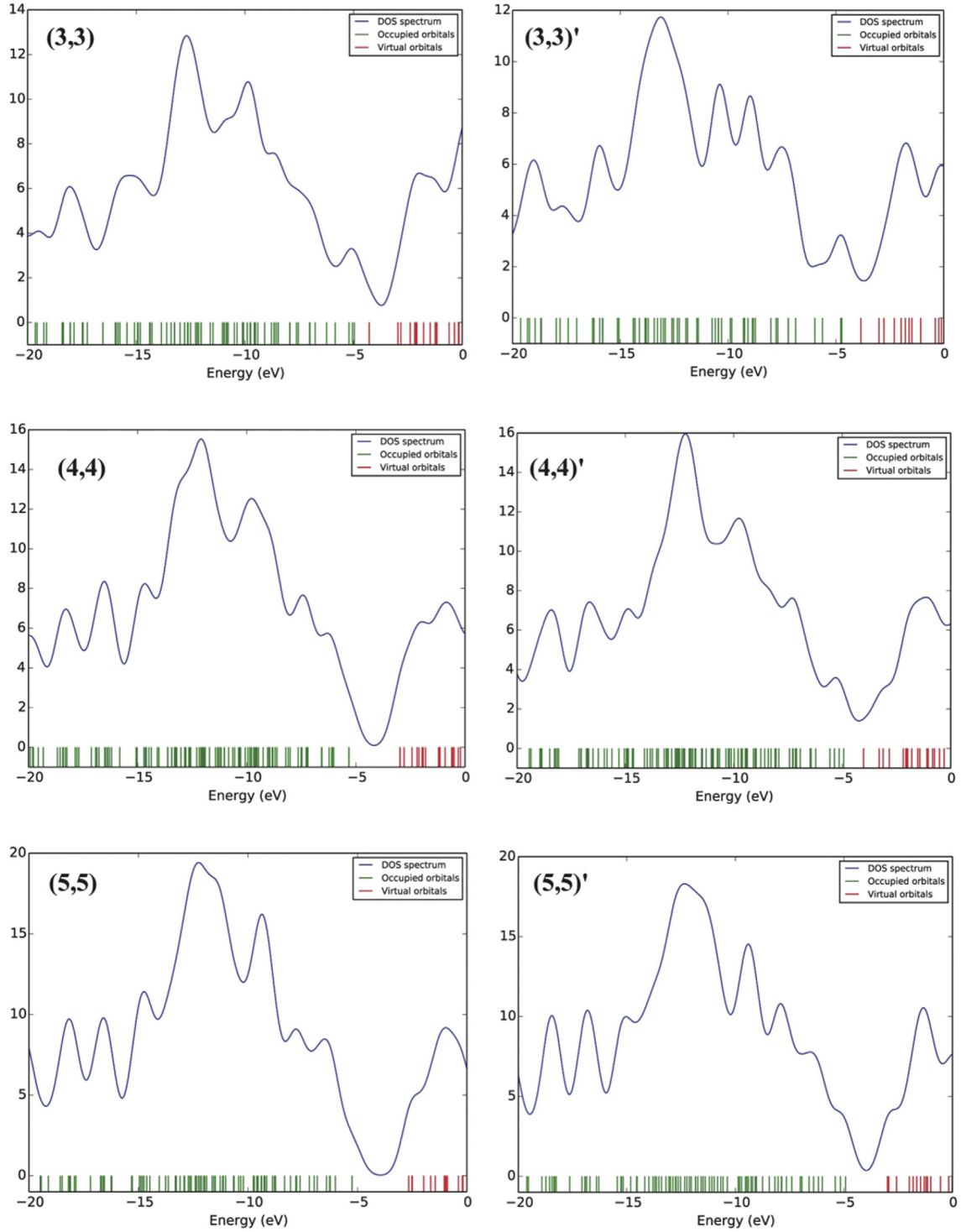

Fig. 7. DOS plots of (*n*,*n*)-SWCNT where n = 3, 4, 5. (A colour version of this figure can be viewed online.)

predicting the possible cap structure for the (3,3), (4,4) and (5,5)-SWCNTs. In the following section we examine the tip electronic structure in order to identity the tip that would be suitable as an STM probe.

3.6. Electronic structure of (n,n)-SWCNT tips (n = 1, 2, 3)

We have calculated the DOS and the MOs at the Fermi level of the various capped SWCNTs in order to find which new cap geometries could serve as STM probes for ultra-high resolution. This was based on (i) the curvature of the electronic distribution of the HOMO at the tip apex, evaluated by the tip asymmetry and (ii) based on the distance that the MOs protrude into the vacuum cap from the surface defined by the nucleus of the carbon atoms in the SWCNT. These DOS plots are presented in Fig. 7 and they show that the (3,3)-SWCNT has a few wavefunctions in the bangap that result in enhanced DOS near the Fermi level. This also applies for the (3,3)' and (4,4)' cap structures, whereas the (4,4), (5,5) and (5,5)' states have a considerable large bangap which results in a zero-DOS at the Fermi level. These DOS plots show that the capped geometries with a single atom at the tip apex (i.e. (3,3)-SWCNT) could potentially be developed in an STM probe for sub-nanometer resolution.

In Fig. 8 we present the HOMO and LUMO of the (3,3)-SWCNT. The HOMO orbital is an extended π-state that covers almost the complete surface of the CNT. This state also extends into the cap region where at the tip apex, comprised of a single carbon atom in trigonal pyramidal configuration, the shape of the wavefunction is of p_z symmetry. This function protrudes into the vacuum gap of the tip-to-surface region vertically to the long axis of the CNT, clearly indicating that if such a tip was applied in STM, the surface state would be interacting with a single wavefunction, which belongs to the conduction band of the CNT. In the case of a positive sample voltage, where tunneling occurs from filled states of the CNT-tip into the empty states of the sample the resolution would therefore be very high. This is based on the spherical-tip approximation by Tersoff-Hamann [27] who showed that the tunneling current exhibits an exponentially decaying dependence on the tip to surface separation (d) and a linear dependence on the bias voltage (V). Furthermore, it was shown analytically that a p_z function at the tip apex would result in extremely high resolution where the tunneling matrix element is proportional to $\partial\Psi/\partial z$ at the nucleus of the apex atom [28]. For a negative sample voltage the (3,3)-SWCNT would not be appropriate to image surface states accurately due to the existence of two lobes of the CNT wavefunction protruding into the tip-to-surface gap, which could result in a double-tip imaging (i.e. superposition of two STM images separated by the distance between the centers of the two lobes). We therefore suggest that the all pentagon cap structure found for the (3,3)-SWCNT should become synthetic targets for the development of high-resolution STM probes.

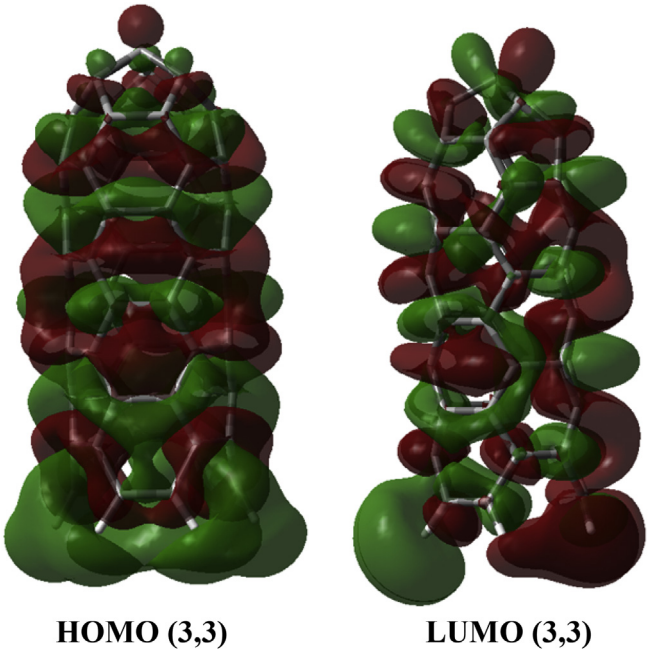

Fig. 8. (a) HOMO and LUMO of (3,3)-SWCNT for an isodensity value of 0.01 C/m^3. (A colour version of this figure can be viewed online.)

4. Conclusion

We applied physical sphere-in-contact models to elucidate the cap geometry of SWCNT with sub-nanometer width (i.e., (3,3), (4,4) and (5,5)-SWCNTs). Detailed hybrid DFT calculations reveal that these new carbon geometries that contain apart from the usual five- and six- member rings, three- and four-member rings which are found to have similar stability to carbon found in other ball-capped zig-zag and arm-chair nanotubes (i.e., (5,5), (6,6), (9,0) and (10,0)) of known stability and synthetic accessibility. We find that the cap structure of the (3,3)-SWCNTs is a pointy carbon geometry comprised of six pentagonal rings with a single carbon atom at the tip apex. In this geometry the carbon atom at the tip apex does not have the usual sp^2 or sp^3 character but a peculiar trigonal pyramidal configuration. DFT calculations of the molecular orbitals and DOS of the tip show that this tip structure apart from being stable can be used in scanning probe microscopies such as STM. It is suggested that these new cap geometries become synthetic targets for the development of STM probes for high resolution imaging.

Acknowledgment

C.D.Z-Y acknowledges funding from EP/L026317/1.

Appendix A. Supplementary data

Supplementary data related to this article can be found at http://dx.doi.org/10.1016/j.carbon.2017.01.074.

References

[1] S.I. Lee, S.W. Howell, A. Ramana, R. Reifenberger, C.V. Nguyen, M. Meyyappan, Complex dynamics of carbon nanotube probe tips, Ultramicroscopy 103 (2005) 95–102.
[2] Y. Shingayaa, T. Nakayamaa, M. Aono, Carbon nanotube tip for scanning tunneling microscopy, Phys. B 323 (2002) 153–155.
[3] A. Pasquini, G.B. Picotto, M. Pisani, STM carbon nanotube tips fabrication for critical dimension measurements, Sens. Actuators A 123–124 (2005) 655–659.
[4] J.R. Sanchez-Valencia, T. Dienel, O. Groning, I. Shorubalko, A. Mueller, M. Jansen, et al., Controlled synthesis of single-chirality carbon nanotubes, Nature 512 (2014) 61–64.
[5] N. Abdurakhmanova, A. Mueller, S. Stepanow, S. Rauschenbach, M. Jansen, K. Kern, et al., Bottom up fabrication of (9, 0) zigzag and (6, 6) armchair carbon nanotube end-caps on the Rh(1 1 1) surface, Carbon 84 (2015) 444–447.
[6] J.A. Morán Meza, C. Lubin, F. Thoyer, K.A. Villegas Rosales, A.A. Gutarra Espinoza, F. Martin, et al., Fabrication of ultra-sharp tips from carbon fiber for scanning tunneling microscopy investigations of epitaxial graphene on 6H-SiC(0 0 0 1) surface, Carbon 86 (2015) 363–370.
[7] J.I. Choi, H.S. Kim, H.S. Kim, G.I. Lee, J.K. Kang, Y.-H. Kim, Carbon nanobuds based on carbon nanotube caps: a first-principles study, Nanoscale 8 (4) (2016) 2343–2349.
[8] H.S. Kim, J. Lee, Y.-H. Kim, Prediction of ultra-high ON/OFF ratio nano-electromechanical switching from covalently-bound C60 chains, Carbon 67 (2014) 48–57.

[9] S.L. Lair, W.C. Herndon, L.E. Murr, S.A. Quinones, End cap nucleation of carbon nanotubes, Carbon 44 (3) (2006) 447–455.
[10] J. Peszke, L. Stobinski, P. Tomasik, K.J. Kurzydlowski, Designing patterns of the isomeric carbon nanotube caps, Phys. Status Solidi (A) Appl. Mater. Sci. 208 (8) (2011) 1801–1803.
[11] J.J. Thomson, The Corpuscular Theory of Matter, Scribner's Sons, New York, 1907, p. 103.
[12] M. Robinson, I. Suarez-Martinez, N.A. Marks, Generalized method for constructing the atomic coordinates of nanotube caps, Phys. Rev. B - Condens. Matter Mater. Phys. 87 (15) (2013).
[13] C. Zeinalipour-Yazdi, D. Pullman, C. Catlow, The sphere-in-contact model of carbon materials, J. Mol. Model (2016) 40.
[14] M.J. Frisch, G.W. Trucks, H.B. Schlegel, G.E. Scuseria MAR, J.R. Cheeseman, G. Scalmani, et al., Gaussian 09, Revision D.01, Gaussian, Inc., Wallingford CT, 2009.
[15] A.D. Becke, Density-functional thermochemistry .3. The role of exact exchange, J. Chem. Phys. 98 (7) (1993) 5648.
[16] C.T. Lee, W.T. Yang, R.G. Parr, Development of the Colle-Salvetti correlation-energy formula into a functional of the electron-density, Phys. Rev. B 37 (2) (1988) 785.
[17] J. Severino, J.-M. Yang, L. Carlson, R. Hicks, Progression of alignment in stretched CNT sheets determined by wide angle X-ray scattering, Carbon 100 (2016) 309–317.
[18] J. Cai, S. Chawla, M. Naraghi, Microstructural evolution and mechanics of hot-drawn CNT- reinforced polymeric nanofibers, Carbon 109 (2016) 813–822.
[19] S. Abouali, M. Akbari Garakani, Z.-L. Xu, J.-K. Kim, $NiCo_2O_4$/CNT nanocomposites as bi- functional electrodes for Li ion batteries and supercapacitors, Carbon 102 (2016) 262–272.
[20] H. Chen, L. Zhang, J. Chen, M. Becton, X. Wang, H. Nie, Effect of CNT length and structural density on viscoelasticity of buckypaper: a coarse-grained molecular dynamics study, Carbon 109 (2016) 19–29.
[21] N. Wang, S. Pandit, L. Ye, M. Edwards, V.R.S.S. Mokkapati, M. Murugesan, et al., Efficient surface modification of carbon nanotubes for fabricating high performance CNT based hybrid nanostructures, Carbon 111 (2017) 402–410.
[22] N.M. O'Boyle, A.L. Tenderholt, K.M. Langner, J. Comp. Chem. 29 (2008) 839–845.
[23] S. Melchor, J.A. Dobado, CoNTub: an algorithm for connecting two arbitrary carbon nanotubes, J. Chem. Inf. Comput. Sci. 44 (2004) 1639–1646.
[24] S.J. Blanksby, G.B. Ellison, Bond dissociation energies of organic molecules, Acc. Chem. Res. 36 (2003) 255–263.
[25] R.M. Silverstein, G.C. Bassler, T.C. Morrill, Spectrometric Identification of Organic Compounds, John Wiley and Sons, New York, 1981.
[26] C.D. Zeinalipour-Yazdi, C. Christofides, Linear correlation between Young's modulus and binding energy in graphene nanoribbons, J. Appl. Phys. 106 (2009) 054318.
[27] J. Tersoff, D.R. Hamann, Theory and application for the scanning tunneling microscope, Phys. Rev. Lett. 50 (25) (1983) 1998–2001.
[28] C.J. Chen, Microscopic view of scanning tunneling miscroscopy, J. Vac. Sci. Technol. 9 (1991) 44–50.

Update

Carbon

Volume 146, Issue , May 2019, Page 369–370

DOI: https://doi.org/10.1016/j.carbon.2019.01.104

Carbon 146 (2019) 369–370

Contents lists available at ScienceDirect

Carbon

journal homepage: www.elsevier.com/locate/carbon

Corrigendum

Corrigendum to “Study of the cap structure of (3,3), (4,4) and (5,5)-SWCNTs: Application of the sphere-in-contact model” [Carbon 115 (2017) 819–827]

Constantinos D. Zeinalipour-Yazdi [a, *], Eriketi Z. Loizidou [b]

[a] Kathleen Lonsdale Materials Chemistry, Department of Chemistry, University College London, London, WC1H 0AJ, UK
[b] Department of Natural Sciences, Middlesex University, Hendon Campus, The Burroughs, London, NW4 4BT, UK

The authors regret that the printed version of the above article contained four incorrect signs in Eqn. (5) which caused the BDE to become negative. The correct and final version follows. The authors would like to apologise for any inconvenience caused.

The change in enthalpy for the bond formation of a PAH from its atoms was calculated based on the following equation

$$\Delta H \cong E_{PAH} - n_C E_C - n_H E_H + ZPV_{PAH} \tag{1}$$

where n_C and n_H is the number of C and H atoms, respectively. E_{PAH}, E_C and E_H are the total energies of the PAH, of an isolated carbon atom in its triplet state and a hydrogen atom in its doublet state and the zero-point vibrational energy (ZPV_{PAH}) was calculated based on,

$$ZPV_{PAH} \cong \frac{hc}{2}\left(\sum_{i=1}^{n_{CC}} \nu_{CC,i} + \sum_{j=1}^{n_{CH}} \nu_{CH,j}\right), \tag{2}$$

where n_{CC} and n_{CH} are the number of C–C and C–H bonds, respectively. Furthermore $\nu_{CC,i}$ and $\nu_{CH,j}$ are the vibrational frequencies of the bonds i and j, respectively, which were calculated via the harmonic oscillator approximation and the finite-difference method. The enthalpy of atomization of the PAH was calculated based on the following relationship,

$$\Delta H_{atom} = n_{CC} BDE_{CC} + n_{CH} BDE_{CH}, \tag{3}$$

where BDE_{CH} and BDE_{CC} are the average bond-dissociation energies of the C–H bond and C–C bond, respectively. The change in enthalpy for the bond formation of the PAH is equal to the negative atomization enthalpy,

$$\Delta H = -\Delta H_{atom}. \tag{4}$$

Therefore after combination of equations (1)–(4), the average BDE per C–C bond in an arbitrary PAH becomes,

$$BDE_{CC} \cong \frac{1}{n_{CC}}\left[-E_{PAH} + n_C E_C + n_H E_H - \frac{hc}{2}\left(\sum_{i=1}^{n_{CC}} \nu_{CC,i} + \sum_{j=1}^{n_{CH}} \nu_{CH,j}\right) - n_{CH} BDE_{CH}\right]. \tag{5}$$

The BDE_{CH} was estimated based on the energy required to dissociate a hydrogen atom from coronene ($R = C_{24}H_{12}$) forming the corresponding radical ($R^{\bullet} = C_{24}H_{11}^{\bullet}$) given by,

$$BDE_{CH} = E_{RH} - E_{R^{\bullet}} - E_{H^{\bullet}} + ZPV_{CH}. \tag{6}$$

DOI of original article: https://doi.org/10.1016/j.carbon.2017.01.074.
* Corresponding author. School of Science, University of Greenwich, Central Avenue, Chatham Maritime, Kent, ME4 4TB, UK.
E-mail address: c.zeinalipouryazdi@greenwich.ac.uk (C.D. Zeinalipour-Yazdi).

https://doi.org/10.1016/j.carbon.2019.01.104
0008-6223/

The average BDE_{CH} for coronene at B3YP/cc-pVDZ(5d,7f) level of theory was found to be 454 kJ mol^{-1} comparable to value reported for the BDE_{CH} in benzene 473 kJ mol^{-1} and methane 439 kJ mol^{-1}. [28] The zero-point vibrational energy (ZPV) of C–H at the same level of theory was found to be 34 kJ mol^{-1} in excellent agreement with the zero-point energy (ZPE) 36 kJ mol^{-1}, calculated from the IR band of the C–H stretching in PAHs located between 3000 and 3100cm^{-1} [29], with the formula given by,

$$ZPE = \hbar\frac{\omega}{2}. \tag{7}$$

The ZPV of C–H was calculated with the following equation,

$$ZPV_{CH} = ZPV_{RH} - ZPV_{R\bullet},$$

where ZPV_{RH} and $ZPV_{R\bullet}$. are the zero-point vibrational energies of coronene and coronene radical in its triplet state calculated at B3YP/cc-pVDZ(5d,7f), respectively.

The average BDE_{CH} of various stable carbon structures and the capped-SWCNT are shown Fig. 6. These calculations show that the stability of planar carbon materials is higher than carbon materials with curved surfaces (e.g. Fullerenes, NC and CNTs). This is associated to the existence of the energy requirements to bend GNR.[30] The bending energy is considerable smaller that the shearing and compression energy as we have previously shown for GNR of varying size. [30] Noteworthy, is that the average BDE_{CC} is correlated to the degree of curvature of the materials shown in Fig. 6. GNR has the highest BDE_{CC} due to its planar structure. This is followed by nanocones (NC) whose energy increases inversely proportional to the tip angle, defined by one of the vertical mirror planes of the $C_{5v}$and C_{4v}, point group symmetries, respectively. The stability of the capped-SWCNT we have examined is intermediate between that of fullerene and the NCs. The most stable capped-SWCNT based on the calculated BDE was the capped (3,3)-SWCNT whereas the least stable was the capped (4,4)-SWCNT due to square geometry at the tip apex.

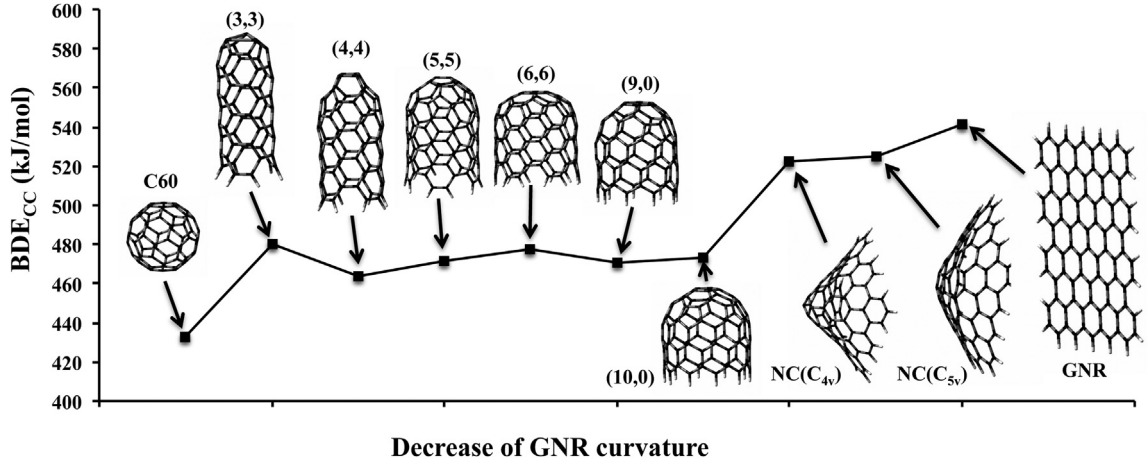

Fig. 6 Stability trends of various carbon materials based on the bond dissociation enthalpy of the C-C bond (BDE_{CC}) calculated by Eqn. (5) as a function of their curvature. Calculations made at B3LYP/cc-pVDZ level of theory.